Robust SHM: Redundancy approach with different sensor integration levels for long life monitoring systems

AUTHORS
(Jan-Hauke BARTELS [1], Thomas POTTHAST [2], Sören MÖLLER [3], Tanja GRIEßMANN [3], Raimund ROLFES [3], Michael BEER [2,4,5], Steffen MARX [1]
[1] Institute of Concrete Structures, TUD Technical University of Dresden, 01219 Dresden, Germany, jan-hauke.bartels@tu-dresden.de
[2] Institute for Risk and Reliability, Leibniz University Hannover, 30167 Hannover, Germany
[3] Institute of Structural Analysis, Leibniz University Hannover, 30167 Hannover, Germany
[4] Institute for Risk and Uncertainty, University of Liverpool, Liverpool L69 7ZF, United Kingdom,
[5] International Joint Research Center for Resilient Infrastructure & International Joint Research Center for Engineering Reliability and Stochastic Mechanics, Tongji University, Shanghai 200092, PR China)

Abstract. Structural health monitoring (SHM) techniques use a variety of sensors, such as displacement, strain, and acceleration sensors, to assess the current condition of engineering structures that are designed to last for decades. Over time, structures can experience degradation-related damage, while the monitoring systems themselves can age and degrade, becoming less reliable. This aging can lead to sensor malfunctions that produce plausible but incorrect data, leading to misinterpretations of structural integrity and potentially catastrophic failures. Therefore, it is critical to distinguish between sensor malfunction and structural anomalies to ensure robust SHM throughout the life cycle of the structure. To address this issue, this study introduces a two-step redundancy approach. First, strain gages were aged in a climate chamber in laboratory experiments to determine the time-variant behavior of the measurement system. Measurement drift and physical gain were identified as significant changes in sensor performance. Second, the redundancy approach using correlation analysis and Gaussian process regression was used to effectively detect and isolate these sensor anomalies. The method successfully distinguished between sensor and structural anomalies and proved to be robust in various scenarios. Further research is suggested to explore the reliability of this approach under conditions where structural and sensor anomalies coincide. This study enhances the robustness of SHM systems and supports reliable assessment of structural health over their lifetime.

Keywords: Acceleratometers, Analytical redundancy, Correlation analysis, Fault detection, Fault diagnosis, Fault isolation, Gaussian process regression, Hardware redundancy, Sensor aging, Sensor integration level, Structural health monitoring, Strain gauges

Introduction

In recent years, the availability and increasing reliability of sensors has led to the increased use of sensors for structural monitoring on complex structural systems such as bridges or wind turbines [1,2]. Structural health monitoring (SHM) techniques can monitor the response of structures to estimate current state of the structure. Various types of sensors with different sensor integration levels, e.g., displacement, strain, and acceleration sensors, provide data for these SHM models. Since engineering structures are designed for a service life of several decades (wind turbines for 20 years, bridges for 100 years), changes occur in the structure, such as deterioration-related damage, and in the environmental conditions such as climate change or changing operational management throughout its life cycle. Monitoring systems must reliably detect these changes. The problem is that, on the one hand, the structure degrades over its lifetime and, on the other hand, the monitoring system itself is subject to an aging process and becomes less reliable [3]. A particular difficulty lies in detecting these sensor malfunctions due to monitoring system aging, as the components of the monitoring system do not fail immediately but gradually deteriorate. At the same time, plausible but faulty data continues to be generated. Using such corrupted data from faulty monitoring systems leads to misinterpretation of structural performance and the possibility of undetected structural damage, which can lead to catastrophic failure. To counteract this problem, basic methods should be used to identify aging phenomena in monitoring systems to ensure robust monitoring systems over the entire service life of the structure. Thus, distinguishing between sensor and structural anomalies is essential for robust SHM systems.

To distinguish between the two, it is important to first understand what a sensor anomaly is. It is defined as a characteristic of the sensor measurement chain where a partial or complete loss of its functionality occurs by recording a data series from the sensor that does not correspond to the actual behavior of the phenomenon in question. [4]. Sensor anomalies can be examined in a system-centric view and a data-centric view [5]. From a system-centric view, sensor anomalies are analyzed based on the root causes of faulty data, which can be categorized into several types, such as calibration malfunctions, connection malfunctions, and low battery. From a data-centric view, sensor anomalies are analyzed based on the features of the measured sensor data; from this perspective, they are generally categorized as successively occurring sensor anomalies and abruptly occurring sensor anomalies. Following the research of Al-Zuriqat et al. in al. [6], Fu et al. in [7] and Lo et al. in [8], data-centric sensor anomalies are mainly categorized into bias, drift, physical gain, outlier, noise and complete failure. In this paper, sensor anomalies are discussed from a data-centric view. **Figure 1** shows typical data-centric sensor anomalies. The successive sensor anomalies in **Figure 1** (**a**) indicate a system in an abnormal or unstable operating condition; the sensor continues to record measurement values, but the data is incorrect [9]. The incorrect readings may be small and change slowly; however, the error gradually increases over a long period and the initially non-critical malfunctions become serious impairments to the measurement system functionality. This type of anomaly is difficult to detect in the initial stage. Successively progressing sensor anomalies are mainly bias, drift and gain. Abruptly occurring sensor anomalies, as depicted in **Figure 1** (**b**), are triggered by physical damage, as a result of which the sensor can no longer function immediately after the anomaly occurs [10]. As these changes are obvious, these anomalies can usually be detected by simple logical considerations. Sensor anomalies that occur abruptly are mainly outliers, noise and electrical short circuits.

Sensor anomalies will change the outcomes of SHM, resulting in false condition assessments. The process of dealing with sensor anomalies is called fault diagnosis. According to [11], fault diagnosis can be described as a process that includes (i) fault detection (presence of fault), (ii) fault isolation (location of fault), (iii) fault identification (type of fault) and (iv) fault adaptation (data reconstruction). This paper focuses on the area of fault detection and isolation. The concept of fault diagnosis has been studied in depth in computer science for several years, e.g., in [12–

14]. Fault identification can be achieved through analytical or hardware redundancy. Physical methods can achieve analytical redundancy. The advantage is that the number of sensors can be minimized. The disadvantage is that it requires an accurate mathematical model of the structure, which is often difficult to obtain. Hardware redundancy is based solely on measurement data without a mathematical model of the structure. Both hardware and analytical redundancy are used in this study to distinguish between different sources of changes in the system.

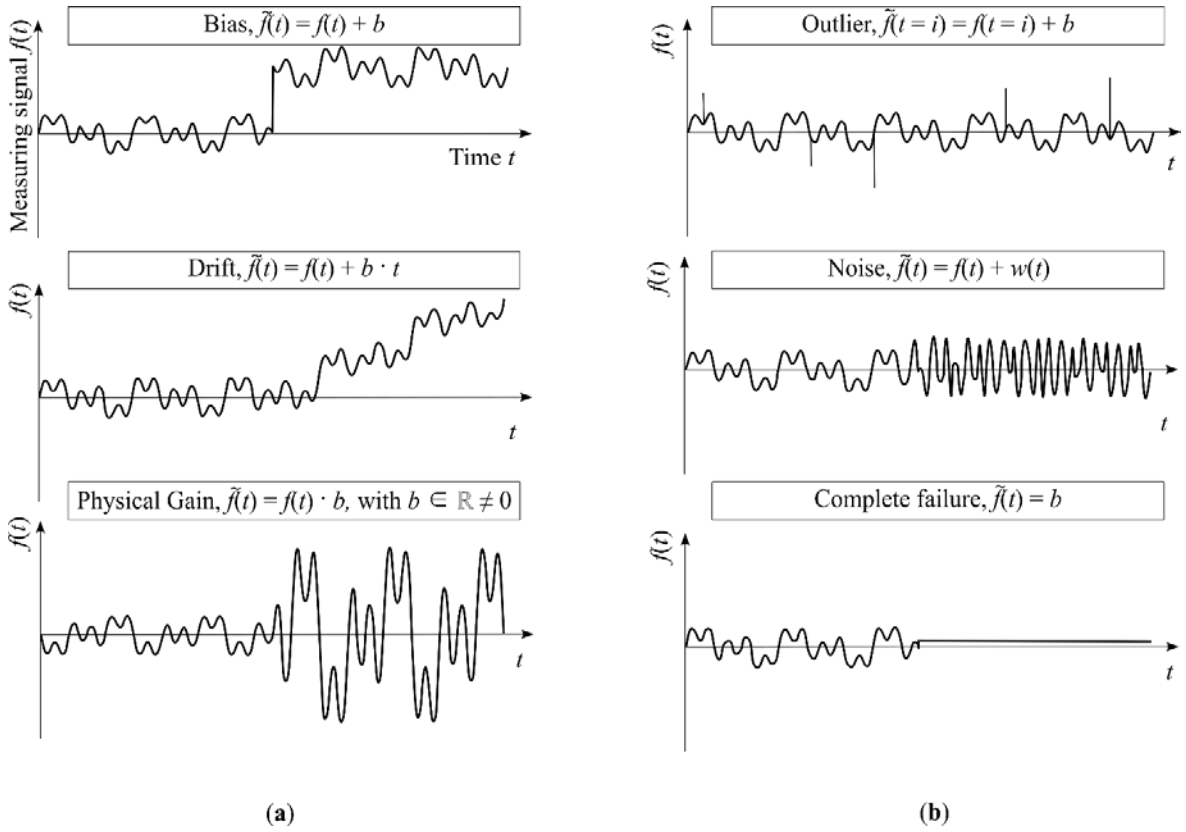

Figure 1. Types of measurement errors. (**a**) Successively occurring sensor malfunction; (**b**) abruptly occurring measurement malfunctions.

Different sensor integration levels (displacement sensors and strain sensors) are used to provide the most reliable values possible within the sensor network.
This paper is organized as follows: First, experimental results of aging measurement systems are presented using strain gauges as an example. In the following, a small-scale clamped beam is modeled. Using the nodes in the finite elements, the discretization points are defined as artificial sensor nodes and supplemented with the real measurement data from the laboratory tests. The method of distinguishing between sensor anomaly and structural damage is explained in the next section. Finally, the paper concludes with a discussion and a future outlook. This paper contributes to more robust monitoring systems. Thanks to interacting sensor nodes, the monitoring system monitors itself and remains reliable over the lifetime of the structure.

Ageing tests with strain gauges

This section describes real aging phenomena that have actually occurred in laboratory tests using strain gauges (SGs) as an example. The tests were carried out at the TU Dresden, Dresden, Germany. The measuring system, consisting of SGs, cable and amplifier, was subjected to a fast-motion aging process by simulating temperature and humidity changes in

a climatic chamber. The test setup, the aging process in the climate chamber, and the time-varying behavior of the measurement system are described and analyzed in the following.

Test setup and measurement technology used

The test setup for the aging tests using the example of the SG measurement chain is shown in **Figure 2**. **Figure 2** (**a**) displays the top view of the realized three-point bending testbet, while **Figure 2** (**b**) visualizes the idealized static system.

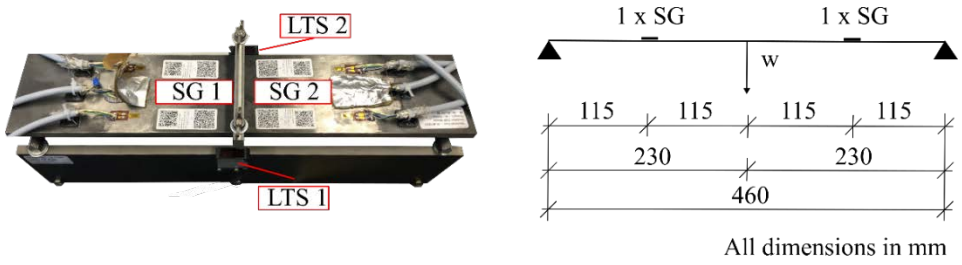

Figure 2. Experimental setup for strain gauges (SGs). (**a**) Top view of the realized setup; (**b**) idealized static system as a three-point bending test.

The test setup consisted of a flat plate mounted on two blade bearings and bent in the center of the field with wing nuts. All components were made of Alloy 36 and bolted together. Alloy 36 is a low-thermal-expansion iron-nickel alloy. Its coefficient of thermal expansion is approximately 26 times less than that of steel. Two SGs were attached to the alloy flat product at each quarter position to measure the strain as the specimen was deformed. In the next step of the experiment, the specimen was subjected to displacement-controlled loading by applying a deflection in the center of the specimen field via wing nuts. The deflection was measured using high-precision laser triangulation sensors (LTS), which have higher accuracy than strain gauges and are therefore suitable for monitoring test performance [15]. A reference measurement was taken at the beginning of the test period at a deflection of 0 mm, a temperature of 20 °C and a relative humidity of 50%. Subsequently, comparison measurements were taken after each aging period. All subsequent comparison measurements were made under identical conditions (0 mm deflection, 20 °C and 50% RH). The aging phenomena for the measurement system was simulated by varying the temperature and humidity in a climate chamber between the comparison measurements. **Figure 3** shows the temperature and humidity cycles that initiate aging process.

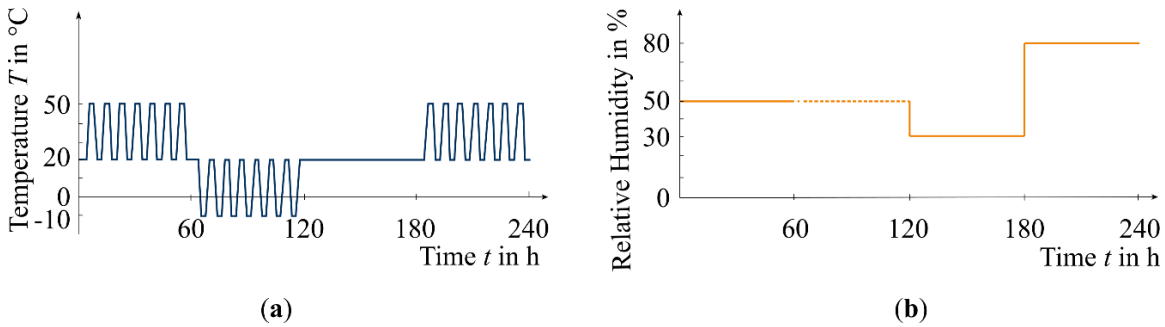

Figure 3. Control of environmental conditions inside the climate chamber. (**a**) Temperature; (**b**) Relative Humidity.

Temperatures and humidity can be divided into four phases. In phase 1, the temperature varied between 20 °C and 50 °C in four-hour cycles, while the relative humidity remained at 50%. In phase 2, the temperature was varied between 20 °C and -10 °C, but the humidity

could not be controlled due to the low temperatures. In phase 3, the temperature and humidity were kept constant at 20 °C and 30%, respectively. Phase 4 showed the same temperature curve as phase 1 but with a higher humidity of 80%. After passing through the four aging phases, a mechanically induced strain measurement was performed to check the functionality of the measuring system.

Test evaluation and test results

The strain change over time was measured to record the time variant behavior of the measurement system. The SGs aged for 282 days. **Figure 4** shows the raw data recorded.

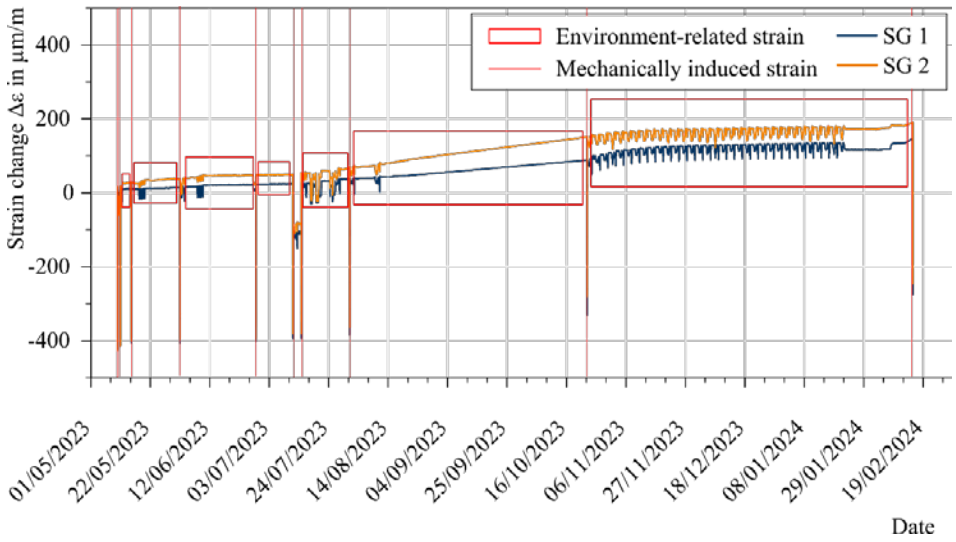

Figure 4. Plot of strain change over time shows the time-variant behavior of strain gauges (SG).

The strains due to changes in temperature and humidity are shown with red rectangles, whereas mechanically induced strains due to deflection of the Alloy 36 material are shown with red lines. Three steps were taken to evaluate the data: (i) The reference test was performed at a sampling rate of 200 Hz for two minutes. The mean value and the twofold standard deviation were calculated as initial reference parameters. (ii) After each environmental aging of the measurement system, a mechanically induced strain test was performed to check the operation of the SGs. (iii) After each mechanically induced strain test, a comparison test was performed with the same boundary conditions as in the first step. A direct comparison with the reference condition is possible using the calculated mean value and twofold standard deviation as comparison parameters. It can be seen in **Figure 4** that there was a drift in the measured value and a physical gain based on theory in depicted in **Figure 1**. The result is approximated by

$$[\bar{\varepsilon}(t)] \pm [\Delta\varepsilon(t)] = \left[4.01 \cdot \sqrt{t}\right] \pm [10.4 + 0.25 \cdot t]. \quad (1)$$

Typically, the measurement result is reported with a mean value $\bar{\varepsilon}$ and a measurement uncertainty $\Delta\varepsilon$ (twofold standard deviation), both assuming linear, time-invariant system characteristics. Since the behavior of the measurement system is obviously time-variant, Equation (1) also takes into account the time dependence of the mean value and the measurement uncertainty via the variable t.

Validation using a monitoring system on a virtual structure

In this section, a simple load-bearing structure is simulated using the finite element method (FEM) and linked to the experimental results mentioned previously. The objective is to develop and validate the concept of distinguishing between sensor and structural anomalies. For this purpose, the data analyzed in the previous section from the aging tests of the SG measurements are used, which occurred in the form of measurement drift and physical gain. Fault detection and fault isolation are performed according to the principle of fault diagnosis.

Construction of the virtual structure with sensor and structural anomalies

The structure modeled by FEM is a clamped cantilever beam with a length of 1.00 m modeled as a flat steel with a cross section of 80 x 12 mm made of S235 steel. The validation setup is shown in **Figure 5**.

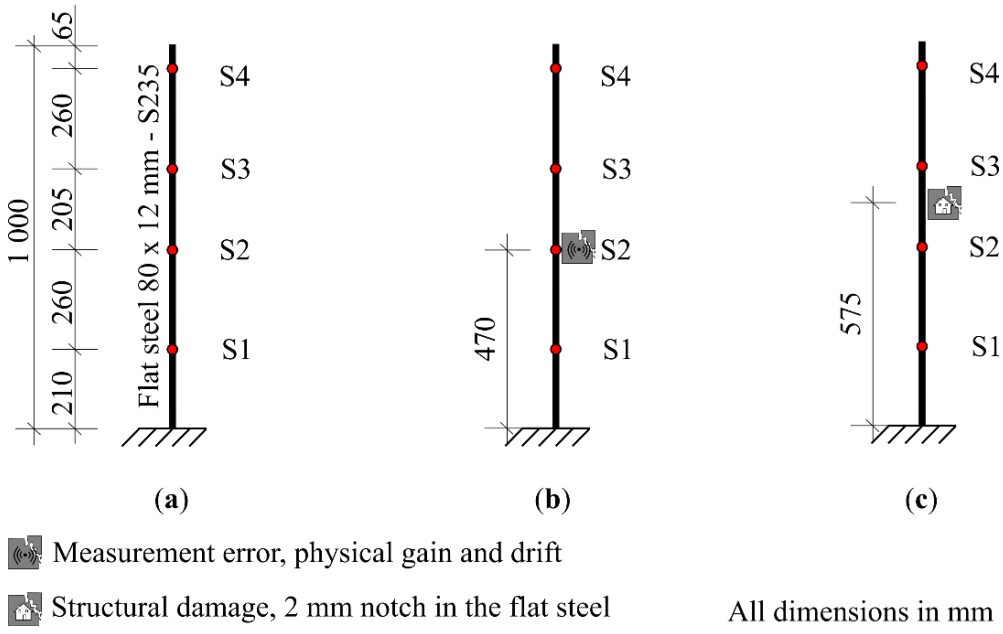

Figure 5. Modeling of a clamped flat steel for the distinction between measurement error and structural damage. (**a**) Without sensor anomaly, without structural anomaly; (**b**) with sensor anomaly in sensor S2, without structural anomaly; (**c**) without sensor anomaly, with structural anomaly between sensors S2 and S3.

The numerical model was discretized in points S1 to S4, whereby the clamping and the free end of the beam were also defined as nodes in the finite element software RSTAB. The structural response is analysed in the discretization nodes; the nodes act as virtual sensors that form the monitoring system for the support structure. The position of sensors S1 to S4 was determined using an optimal sensor placement algorithm based on the Effective Independence Method. Here, the model was discretized by a dense mesh, whereby each node was a possible sensor position and was evaluated concerning its information quality for determining the eigenform. The aim was to minimize the number of sensor positions without reducing the information quality of the monitoring system too much. For example, further information on optimal sensor placement using the Effective Independence Method can be found in [16].

There are three different states for the validation. **Figure 3** (**a**) shows the undamaged condition of the structure and the monitoring system. This state is used as a reference basis. **Figure 3** (**b**) shows the change in the state of the monitoring system by simulating a sensor anomaly in sensor S2. The sensor anomaly is applied as measurement drift and a physical gain in the order of magnitude as measured in the actual SG experiments. **Figure 3** (**c**) shows the change of the state in the structure with a structural anomaly. For this purpose, a cross-

section reduction from 12 mm to 10 mm width is modeled to simulate a crack in the steel cross-section.

Data acquisition with synthetically generated measurement data

The system is subjected to a dynamic load described by a Diraq impulse; the system response is then recorded over a period of 60 seconds. **Figure 6** shows the dynamic excitation of the system and the system response over time.

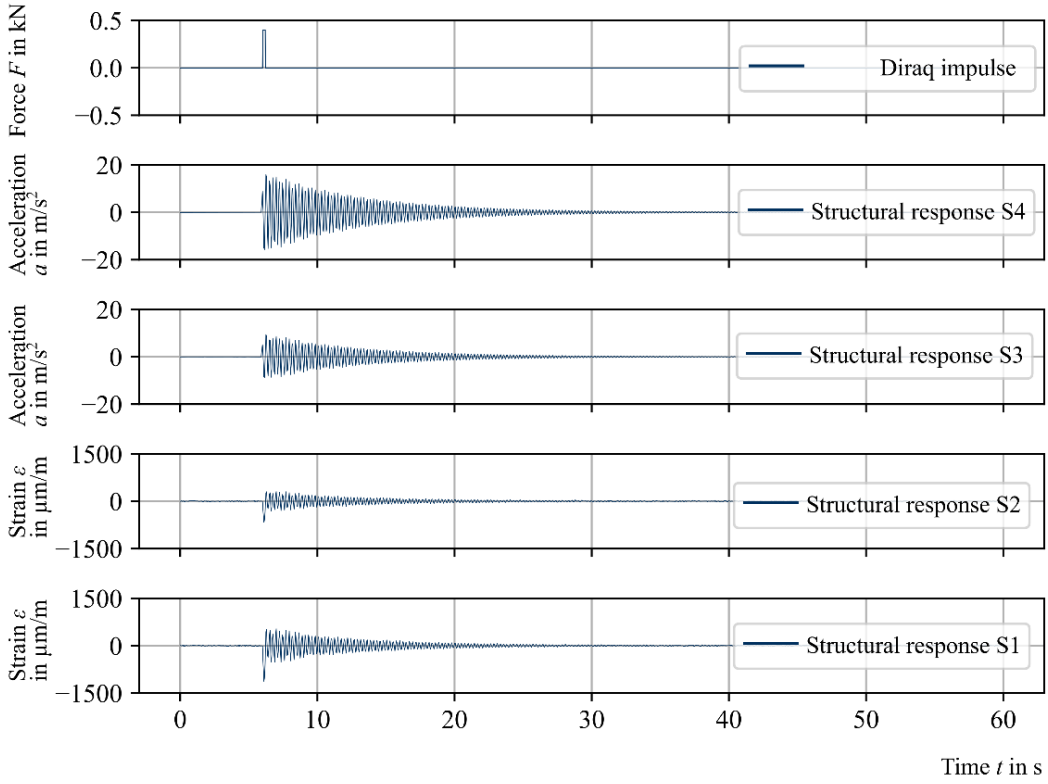

Figure 6. Excitation of the system and system response using a virtual monitoring system of the undamaged state with normally distributed noise (twofold standard deviation) over time; Diraq impulse as excitation of the system; structural response of system in S4 in m/s²; structural response of system in S3 in m/s²; structural response of system in S2 in µm/m; structural response of system in S1 in µm/m

The physical quantities exported from the finite element software were the horizontal deflection u_z in mm and the horizontal vibration acceleration a in m/s². This data package forms the raw data basis for further evaluation. As the laboratory tests were carried out with strain gauges, the horizontal deflection must be converted into an equivalent strain ε in µm/m using a transfer function. Assuming the following aspects:

- the force is applied at the free end of the beam,
- there is a plane bending,
- the cross-section remains flat (Bernoulli hypothesis), and
- the material is isotropic and homogeneous (Hooke's law),

the beam theory is used to describe the mechanical behaviour. Based on this, the transfer function from displacement to strain can be calculated using

$$\varepsilon(x) = \frac{6 \cdot (x - l) \cdot z \cdot w(x)}{x^3 + (l \cdot x^2 \cdot 3)}. \tag{2}$$

Here, $\varepsilon(x)$ is the strain in µm/m, w is the horizontal deflection of the vertical cantilever in mm, l is the length of the cantilever, and z is the distance from the center of mass to the edge of the component (cross-sectional point at which the strain gauge is used for measurement). The structural responses in the individual sensor positions show different sensor integration levels. Strain gauges are used in S1 and S2 to measure the strain, while acceleration sensors are used in S3 and S4 to measure the acceleration. The reason for this is that the signal-to-noise ratio of the respective sensors is maximized in the raw data signal so that the noise will have less influence on the measurement signal analysis. The actual signal-to-noise of the SGs used is added to the raw data from the laboratory tests described above. The actual signal-to-noise ration of the acceleration sensors is added to the raw data signal based on the work in [17]. With this database for all three states from **Figure 5**, the method for distinguishing between sensor and structural anomalies is carried out in the next section.

Is it a sensor or structural anomaly?

A two-stage redundancy approach is developed to answer this question: (i) Fault detection of a sensor anomaly using a hardware redundancy approach via the correlation between sensors of different integration levels; (ii) Fault isolation using an analytical redundancy approach via Gaussian processes (GP) within the respective sensor over time.

Fault detection using hardware redundancy

A good framework for sensor fault detection should be robust against noise. Therefore, different levels of sensor integration were used within the monitoring system to maximize the signal-to-noise ratio. In areas where horizontal deflection is minimal, strain is maximized. SGs are used there. In areas where horizontal deflection is at its maximum, the vibration acceleration is at its peak as well. Thus, accelerometers are used at this position. The sensor anomaly (**Figure 5** (**b**)) can be distinguished from the structural anomaly (**Figure 5** (**c**)) by comparison with the reference state in **Figure 5** (**a**). For this purpose, the correlation matrix of the sensor network is set up and the frobenius scalar product (FSB) changes in the three states are observed. The FSB is a scalar product on the vector space of real or complex matrices. It is calculated by squaring the entries in the matrix, component by component, and then summing over all these products. The result is shown in **Figure 7**.

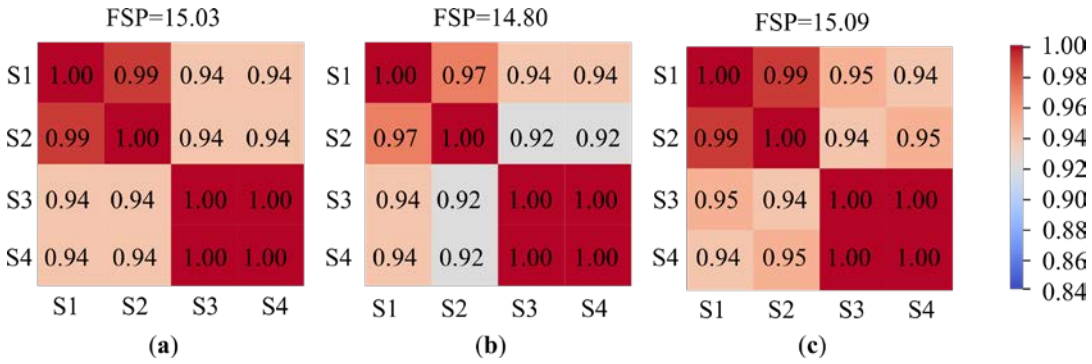

Figure 7. Comparison of the correlation matrices and the frobenius scalar product (FSP). (**a**) Without sensor anomaly, without structural anomaly; (**b**) with sensor anomaly in sensor S2, without structural anomaly; (**c**) without sensor anomaly, with structural anomaly between sensors S2 and S3.

It can be seen that the FSB of case (**b**) is significantly lower than the FSB of the other two cases (**a**) and (**c**). This indicates a sensor anomaly, because one sensor within the sensor network is no longer as strongly correlated with the other sensors, and thus the FSB becomes

smaller. The structural anomaly shows a change in the measurement signal in all sensors, so the correlation between the individual sensors within the sensor network remains the same.

Fault isolation using analytical redundancy

For fault isolation, the second step is to select a method that can be used to identify the faulty sensor in the sensor network. For this purpose, an analytical redundancy approach using gaussian process regression (GPR) is chosen. Instead of installing multiple sensors to measure a single parameter, the analytical redundancy approach uses the information inherent in the SHM system. It takes advantage of the correlation between the regularly installed sensors [12]. For each observed sensor, virtual sensor outputs representing fault-free operation are predicted based on the measured outputs of correlated sensors and a priori knowledge of the system. By comparing the actual and virtual sensor outputs, residuals are generated for each sensor. The residuals, which reflect inconsistencies between the actual sensor behavior and the model-based virtual sensor behavior, serve as a basis for decision-making regarding possible fault isolation. In this work, a GP was chosen to determine the mathematical model. The GP was trained on the correlating sensors S1 through S4. More information about GPR can be found, e.g., in [18]. Four models were trained, with one sensor selected as output and the three remaining sensors as input in each model. Before training the GPR models for FD, the measurements were split into 75% training and 25% testing data sets. This avoids overfitting the model. The results of the four models are shown in **Table 1**.

Table 1. Fault isolation within the monitoring system for sensors S1 to S4 using the coefficient of determination R^2 and the mean absolute error (MAE).

	Input: S2, S3, S4 Output: S1	Input: S1, S3, S4 Output: S2	Input: S1, S2, S4 Output: S3	Input: S1, S2, S3 Output: S4
R^2	0.97	0.83	0.99	0.99
MAE	14.49	22.65	0.03	0.03

It can be seen that the coefficient of determination R^2 is lowest for sensor S2, while the mean absolute error (MAE) is highest for sensor S2. It is clear that the MAE value for output sensor S1 and output sensor S2 is comparatively high compared to the other two output variants S3 and S4. This is because the noise in the S1 and S2 outputs comes from the SGs and the noise in the S3 and S4 outputs comes from the accelerometers used. Since the signal-to-noise ratio of the accelerometers is higher than that of the SGs, the MAE is significantly lower for the accelerometer outputs. Overall, except for output S2, all models show good agreement and small approximation errors, so it can be confidently stated that sensor S2 is subject to a sensor anomaly. This can be confirmed with the initial situation in **Figure 5** (**b**).

Conclusion and Outlook

Sensor anomalies in SHM systems can reduce the monitoring quality and cause significant economic loss due to inaccurate measurement data required for the structural assessment of the monitored structure. However, fault detection and isolation in SHM systems have received little attention. Therefore, this paper presented a two-step process to distinguish between sensor and structural anomalies. First, laboratory experiments were conducted using strain gauges. The sensors were aged using temperature and humidity in a climatic chamber to see which aging phenomena were detectable in the measurement signal. It was found that measurement drift and physical gain cause a significant change in the measurement signal, which could be detected and isolated using a two-stage redundancy approach. Correlation

analysis between sensors of different integration levels (hardware redundancy) was used for fault detection. For fault isolation, individual sensors were considered over time, and a gaussian process was used to evaluate how well the current sensor behavior matched the sensor's reference state. The approach proved reliable in detecting and isolating sensor anomalies and distinguishing between sensor and structural anomalies. Future studies need to investigate whether the approach is also reliable when the structural anomaly is close to a sensor position or when a structural anomaly and a sensor anomaly coincide. Nevertheless, the validation on a virtual structural system already shows that the approach presented here can increase the robustness of SHM systems. The method enhances the monitoring of load-bearing structures over their lifetime and ensures a reliable structural condition assessment.

Acknowledgements

This research was funded by the German Research Foundation (DFG), as part of the Collaborative Research Centre 1463 (SFB 1463) “Integrated Design and Operation Methodology for Offshore Megastructures” (project number 434502799). This article represents the opinions of the authors and does not mean to represent the position or opinions of the funding entities.

References

[1] Botz, M. et al. (2016). Monitoring of wind turbine structures with concrete-steel hybrid-tower design. *Proceedings of the 8th European Workshop on Structural Health Monitoring (EWSHM), Bilbao, Spain*.

[2] Gatti, M. (2019). Structural health monitoring of an operational bridge: A case study. *Engineering Structures*. DOI: 10.1016/j.engstruct.2019.05.102.

[3] Bartels, J.-H. et al. (2023). Robust SHM Systems Using Bayesian Model Updating.

[4] Bayar, N. et al. (2015). Fault detection, diagnosis and recovery using Artificial Immune Systems: A review. *Engineering Applications of Artificial Intelligence*. DOI: 10.1016/j.engappai.2015.08.006.

[5] Ni, K. et al. (2009). Sensor network data fault types. *ACM Transactions on Sensor Networks*. DOI: 10.1145/1525856.1525863.

[6] Al-Zuriqat, T. et al. (2023). Adaptive Fault Diagnosis for Simultaneous Sensor Faults in Structural Health Monitoring Systems. *Infrastructures*. DOI: 10.3390/infrastructures8030039.

[7] Fu, Y. et al. (2019). Sensor fault management techniques for wireless smart sensor networks in structural health monitoring. *Structural Control and Health Monitoring*. DOI: 10.1002/stc.2362.

[8] Lo, C. et al. (2015). Efficient Sensor Fault Detection Using Group Testing. DOI: 10.48550/arXiv.1501.04152.

[9] Wang, Y. et al. (2016). Wavelet-Based Feature Extraction in Fault Diagnosis for Biquad High-Pass Filter Circuit. *Mathematical Problems in Engineering*. DOI: 10.1155/2016/5682847.

[10] Samara, P. et al. (2008). A Statistical Method for the Detection of Sensor Abrupt Faults in Aircraft Control Systems. *IEEE Transactions on Control Systems Technology*. DOI: 10.1109/TCST.2007.903109.

[11] Patton, R. (1991). Fault detection and diagnosis in aerospace systems using analytical redundancy. *Computing & Control Engineering Journal*. DOI: 10.1049/cce:19910031.

[12] Smarsly, K. and Law, K. (2014). Decentralized fault detection and isolation in wireless structural health monitoring systems using analytical redundancy. *Advances in Engineering Software*. DOI: 10.1016/j.advengsoft.2014.02.005.

[13] Jana, D. et al. (2022). CNN and Convolutional Autoencoder (CAE) based real-time sensor fault detection, localization, and correction. *Mechanical Systems and Signal Processing*. DOI: 10.1016/j.ymssp.2021.108723.

[14] Kullaa, J. (2011). Distinguishing between sensor fault, structural damage, and environmental or operational effects in structural health monitoring. *Mechanical Systems and Signal Processing*. DOI: 10.1016/j.ymssp.2011.05.017.

[15] Bartels, J.-H. et al. (2023). Einflüsse auf die Messunsicherheit von SHM–Systemen und deren Kompensation am Beispiel von Laser–Distanzmessungen. *Bautechnik*. DOI: 10.1002/bate.202200102.

[16] Hassani, S. and Dackermann, U. (2023). A Systematic Review of Optimization Algorithms for Structural Health Monitoring and Optimal Sensor Placement. *Sensors*. DOI: 10.3390/s23063293.

[17] Bartels, J.-H. et al. (2024). Experimental Investigation on the Transfer Behavior and Environmental Influences of Low-Noise Integrated Electronic Piezoelectric Acceleration Sensors. *Metrology*. DOI: 10.3390/metrology4010004.

[18] Wang, J. (2023). An Intuitive Tutorial to Gaussian Process Regression. *Computing in Science & Engineering*. DOI: 10.1109/MCSE.2023.3342149.